

Ultraheavy Ultrahigh-Energy Cosmic Rays

B. Theodore Zhang¹, Kohta Murase^{2,3,4,1}, Nick Ekanger⁵, Mukul Bhattacharya^{2,3,4}, Shunsaku Horiuchi^{5,6}

¹*Center for Gravitational Physics and Quantum Information,*

Yukawa Institute for Theoretical Physics, Kyoto University, Kyoto, Kyoto 606-8502, Japan

²*Department of Physics, The Pennsylvania State University, University Park, PA 16802, USA*

³*Department of Astronomy & Astrophysics, The Pennsylvania State University, University Park, PA 16802, USA*

⁴*Center for Multimessenger Astrophysics, Institute for Gravitation and the Cosmos,
The Pennsylvania State University, University Park, PA 16802, USA*

⁵*Center for Neutrino Physics, Department of Physics, Virginia Tech, Blacksburg, VA 24061, USA and*

⁶*Kavli IPMU (WPI), UTIAS, The University of Tokyo, Kashiwa, Chiba 277-8583, Japan*

(Dated: June 13, 2024)

We investigate the propagation of ultraheavy (UH) nuclei as ultrahigh-energy cosmic rays (UHECRs). We show that their energy loss lengths at $\lesssim 300$ EeV are significantly longer than those of protons and intermediate-mass nuclei, and that the highest-energy cosmic rays with energies beyond ~ 100 EeV, including the Amaterasu particle, may originate from such UH-UHECRs. We derive constraints on the contribution of UH-UHECR sources, and find that they are consistent with energy generation rate densities of UHECRs from collapsars and neutron star mergers.

INTRODUCTION

The origin of ultrahigh-energy cosmic rays (UHECRs) has been a long-standing mystery for over 50 years since the first detection of ~ 100 EeV cosmic rays (see reviews, Refs. [1–4]). The observed spectrum of UHECRs shows a hardening at the ankle around 4 EeV and a cutoff at ~ 50 EeV [5–7]. There are possible discrepancies in the measured energy spectra [8] between the Pierre Auger Observatory (Auger) [9] and Telescope Array (TA) [10, 11] observations. Even though the differences at low energies may be explained by the systematic effect on the energy scale, an excess remains in the TA data at the highest energies [12]. Recently, TA reported the detection of an extremely energetic UHECR event with the energy of $244 \pm 29(\text{stat.})_{-76}^{+51}(\text{syst.})$ EeV, dubbed the “Amaterasu” particle [13].

The composition of UHECRs is important to unveil their origin (see e.g., Ref. [14]). The depth of the cosmic-ray shower maximum, X_{max} , is a measurable quantity used to infer the particle composition [15]. The Auger data favor a mixed composition of UHECRs, and intermediate-mass (e.g., carbon and oxygen) and/or heavy (e.g., iron) nuclei make significant contributions beyond 10 EeV [16–18]. In particular, the fraction of protons gradually decreases above the ankle, while intermediate-mass nuclei may become dominant at higher energies. The contribution of heavy nuclei seems negligible within the energy range of $10^{18.4} - 10^{19.4}$ eV [18], but these results are largely affected by hadronic interaction models. The distribution of X_{max} measured by TA is consistent with the Auger data, but the interpretation is still under debate [19].

Not all UHECR source candidates can dominantly generate heavy nuclei as UHECRs. Production and acceleration of heavy nuclei has been considered in the context of collapsars [20–29] and compact binary mergers

involving a neutron star [30–34]. The energy generation rate density of UHECRs at $10^{19.5}$ eV is $EQ_E^{19.5} \approx (0.2 - 2) \times 10^{43}$ erg Mpc⁻³ yr⁻¹ (e.g., Refs. [35, 36]), which is consistent with the energy budget of collapsars including gamma-ray bursts (GRBs) and hypernovae, as well as binary neutron star (BNS) mergers (see Table II of Ref. [34]). With the luminosity requirement [37] obtained from the Hillas condition [1], the maximum possible energy of the accelerated cosmic rays is estimated to be

$$E_{A,\text{max}} \approx 9.8 \times 10^{20} \text{ eV} \left(\frac{Z}{40} \right) \left(\frac{\epsilon_B}{0.01} \right)^{1/2} \times \left(\frac{L}{10^{51} \text{ erg/s}} \right)^{1/2} \left(\frac{\Gamma}{10^{2.5}} \right)^{-1} \beta^{1/2} \quad (1)$$

where Z is the nuclei charge, ϵ_B is the energy fraction of the magnetic field, L is the total luminosity, Γ is the Lorentz factor, and β is the characteristic velocity normalized by the speed of light.

Ultraheavy (UH) nuclei, which are defined as nuclei heavier than iron-group nuclei throughout this work, are believed to be synthesized due to the r -process occurring inside neutron-rich environments [38–43]. The sources of UH nuclei can be BNS and neutron-star–black-hole (NSBH) mergers (e.g., Refs. [44–48]), as well as collapsars including GRBs and magnetorotational supernovae (e.g., Refs. [23, 29, 49–55]). UH nuclei have the advantage of being accelerated to energies beyond 100 EeV, compared to conventional light- and intermediate-mass group nuclei, which could provide an additional contribution to the highest-energy cosmic rays.

In this work, we study the fate of UH-UHECRs during their intergalactic propagation and constrain their contributions to the highest-energy cosmic rays with energies exceeding 10^{20} eV. We also discuss the plausibility of the Amaterasu particle as an UH-UHECR event and its implications for future observations.

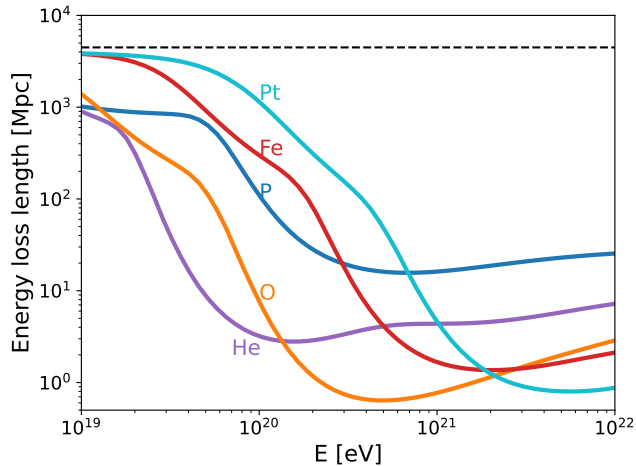


FIG. 1. Total energy loss lengths for various nuclei: p, He, O, Fe, and Pt. The black dashed line is the energy loss length due to the adiabatic expansion of the universe. CMB and EBL [60] are considered as target photons.

PROPAGATION OF UH-UHECRS

UH nuclei can be photodisintegrated and spalled into lighter nuclei due to their interactions with background target photons and matter, respectively. For the propagation of UHECRs from their source to Earth, interactions with the cosmic microwave background (CMB) and extragalactic background light (EBL) are dominant, and we utilize the public code CRPROPA 3.2 to propagate UHECRs through intergalactic space [56]. However, because CRPROPA 3.2 does not provide a module for nuclei with mass numbers of $A > 56$, we newly generate the photodisintegration cross section table of UH-UHECRs using the nuclear reaction network TALYS 1.96 [57, 58] as an extension to CRPROPA 3.2. In our photodisintegration reaction network, the maximum atomic number and mass number of nuclei are $Z = 92$ and $A = 146$, respectively, with a total of 2434 isotopes. In addition, the decay of unstable UH-UHECRs is implemented with the data table taken from NUDAT 3 [59].

The dominant energy loss processes during the intergalactic propagation of UHECR nuclei are photodisintegration, photomeson production, Bethe-Heitler pair production, and adiabatic losses due to the cosmic expansion. In Fig. 1, we show total energy loss lengths for light nuclei represented by proton (p) and helium (He), oxygen (O) as intermediate-mass nuclei, iron (Fe) as heavy nuclei, and platinum (Pt) as UH nuclei. See Supplementary Material (SM) for other representative UH nuclei. The inverse of the total energy loss length is written as $\lambda_{\text{loss}}^{-1} = \lambda_{\text{loss,phdis}}^{-1} + \lambda_{\text{loss,phmes}}^{-1} + \lambda_{\text{loss,BH}}^{-1} + \lambda_{\text{loss,ad}}^{-1}$, where $\lambda_{\text{loss,ad}} = c/H_0 \sim 4000$ Mpc is the adiabatic energy loss length. The photodisintegration energy loss length is $\lambda_{\text{loss}}^{\text{phdis}} \approx (n_{\text{CMB}} \hat{\sigma}_{\text{phdis}})^{-1} \simeq$

$1.3(A/195)^{-0.21}$ Mpc, where $\hat{\sigma}_{\text{dis}} = \sigma_{A\gamma} \kappa_{A\gamma}$ is the effective photodisintegration cross section and $\kappa_{A\gamma} \approx 1/A$ is the inelasticity at the giant dipole resonance (GDR) [61, 62]. The effective photodisintegration cross section for UH nuclei can be analytically approximated as $\sigma_{A\gamma} \approx \sigma_{\text{GDR}} \Delta \bar{\varepsilon}_{\text{GDR}} / \bar{\varepsilon}_{\text{GDR}} \approx 120(A/195)^{1.21}$ mb for $A \gtrsim 10$, where $\sigma_{\text{GDR}} \approx 4.3 \times 10^{-28} A^{1.35}$ cm² is the GDR cross section, $\Delta \bar{\varepsilon}_{\text{GDR}} \approx 21.05 A^{-0.35}$ MeV is the width [63], and $\bar{\varepsilon}_{\text{GDR}} \approx 42.65 A^{-0.21}$ MeV is the resonance energy in the nuclear rest frame [64, 65]. The typical resonance energy is $E_A^{\text{phdis}} \approx 0.5 A m_p c^2 \bar{\varepsilon}_{\text{GDR}} / \varepsilon_t \simeq 1.9 \times 10^{21}$ eV $(A/195)^{0.79} (\varepsilon_t / 6.6 \times 10^{-4} \text{ eV})^{-1}$, where ε_t is the target photon energy. Energy losses due to the Bethe-Heitler pair production process are also important for UH-UHECRs because of their large atomic numbers. The energy loss length is estimated to be $\lambda_{\text{loss}}^{\text{BH}} \approx (n_{\text{CMB}} \hat{\sigma}_{\text{BH}})^{-1} \simeq 32 (Z/78)^{-2} (A/195)$ Mpc, where $\hat{\sigma}_{\text{BH}} \sim 8 \times 10^{-31} (Z^2/A)$ cm² is the effective cross section [22, 66], $E_A^{\text{BH}} \approx 0.5 A m_p c^2 \bar{\varepsilon}_{\text{BH}} / \varepsilon_{\text{CMB}} \simeq 1.4 \times 10^{21}$ eV $(A/195) (\varepsilon_t / 6.6 \times 10^{-4} \text{ eV})^{-1}$ is the typical energy, and $\bar{\varepsilon}_{\text{BH}} \sim 10$ MeV. Although the photodisintegration process is expected to be dominant, which is indeed the case at $E_A \sim$ a few $\times 10^{21}$ eV, we find that the Bethe-Heitler pair production process is the most important at $E_A \sim (1-5) \times 10^{20}$ eV (see Fig. 5 in SM). The photomeson production process is irrelevant when considering the propagation of UH-UHECRs due to the high-energy threshold at $\sim 4 \times 10^{22}$ eV $(A/195) (\varepsilon_t / 6.6 \times 10^{-4} \text{ eV})^{-1}$.

As seen in Fig 1, UH-UHECRs can travel longer distances than the GZK (Greisen-Zatsepin-Kuzmin) distance for UHECR protons [67, 68] and the energy loss length of iron-group-mass nuclei [61, 62, 69, 70]. Thanks to their large mass numbers, it takes longer for them to be completely disintegrated, by which rarer sources can contribute or UH-UHECRs could appear beyond the cutoff in spectra of UHECR protons and conventional nuclei. To calculate the UHECR spectrum and composition on Earth, we take into account the change in the composition of UH-UHECRs during propagation, as the UH nuclei become progressively lighter with the ejection of one or more nucleons (see SM for details).

UH-UHECR SPECTRUM AND COMPOSITION

Using the available Auger and TA data for the energy spectrum and composition of UHECRs, we examine possible contributions of the sources of UH-UHECRs. For the demonstration, we consider two representative composition models of conventional nuclei, depending on whether there are heavy iron-group nuclei or not:

- *Model A*: conventional nuclei (p, He, O, Si) + UH nuclei (Se, Te, Pt)
- *Model B*: conventional nuclei (p, He, O, Si, Fe) + UH nuclei (Se, Te, Pt)

The origin of intermediate-mass nuclei can be associated with material from the inner core of massive stars collapsing into black holes [27, 71]. Iron-group nuclei are naturally expected in the supernova/hypernova ejecta [20, 21, 24, 25, 27, 29] or the surface of neutron stars [72, 73]. Alternatively, UHECR nuclei can be provided by the reacceleration of Galactic cosmic rays [74, 75]. We treat UH-UHECRs as an additional component, assuming that they are produced by either the same or different populations. We consider Selenium (Se), Tellurium (Te), and Pt to represent the first, second, and third peaks of UH nuclei synthesized via the r -process.

The injection spectrum of UHECRs escaping from the sources is assumed to be a power law with an exponential cutoff,

$$\frac{d\dot{N}_A}{d\mathcal{R}} = f_A \dot{N}_0 \left(\frac{\mathcal{R}}{\mathcal{R}_0} \right)^{-s_{\text{CR}}} \exp \left(-\frac{\mathcal{R}}{\mathcal{R}_{\text{max}}} \right), \quad (2)$$

where $\mathcal{R} = E/Z$ is particle rigidity, E is particle energy, Z is nuclear charge number, \mathcal{R}_0 is a reference rigidity, f_A is the number fraction of nuclei, s_{CR} is the spectral index, and \dot{N}_0 is a normalization constant. To reduce the number of free parameters, we assume all of the accelerated nuclei have the same rigidity, \mathcal{R}_{max} , and the spectral index, s_{CR} . We also assume no redshift evolution for the sources, which is sufficient for our purpose to constrain the contribution of UH-UHECRs. Large-scale magnetic fields in structured regions of the Universe could further modify the observed spectrum and composition, whereby cosmic rays with low rigidities cannot arrive on Earth, also known as the magnetic horizon effect [80, 81]. However, this effect is important only if the average source separation is $d_s \gtrsim 20\sqrt{l_c}/0.1$ Mpc Mpc, where l_c is the coherence length [82]. Because transient sources like collapsars and BNS mergers may lead to sufficient source densities [83, 84], it is reasonable to adopt the one-dimensional propagation scenario assuming UHECR sources have an average distance less than 20 Mpc. In this work, we adopt the hadronic interaction model EPOS-LHC [14, 85].

To constrain the energy generation rate density of UH-UHECRs, $Q_{\text{UH-UHECR}} \equiv \int_{E_{\text{min}}}^{E_{\text{max}}} dRE \frac{d\dot{N}_A}{d\mathcal{R}}$ with $E_{\text{min}} = 10^{18}$ eV and $E_{\text{max}} = 10^{21}$ eV (cf. Ref. [86]), we perform a combined fit with both conventional and UH nuclei components. For simplicity, we only consider the combination of conventional nuclei with one of the UH nuclei, among Se, Te, and Pt, for both *Model A* and *Model B*, which allows us to explore the effect of mass and charge of UH nuclei on the derived fit. For the TA data, we show the best-fit values of the energy generation rate density of UH-UHECRs, where the uncertainty is estimated under the condition that the total chi-square value $\chi_{\text{tot}}^2 \leq \chi_{\text{tot,min}}^2 + 1$. For the Auger data, we use $\chi_{\text{tot}}^2 \leq \chi_{\text{tot,min}}^2 + 10$ to estimate the uncertainty range

Nuclei	$Q_{\text{UH-UHECR}}^{\text{Auger}}$ [erg Mpc ⁻³ yr ⁻¹]	$Q_{\text{UH-UHECR}}^{\text{TA}}$ [erg Mpc ⁻³ yr ⁻¹]
<i>Model A</i>		
Se	$14.4_{-6.1}^{+0.7} \times 10^{42}$	$4.1_{-1.7}^{+1.6} \times 10^{43}$
Te	$3.0_{-0.9}^{+4.3} \times 10^{42}$	$2.2_{-0.6}^{+0.8} \times 10^{43}$
Pt	$2.3_{-1.4}^{+3.2} \times 10^{42}$	$1.8_{-0.4}^{+0.6} \times 10^{43}$
<i>Model B</i>		
Se	$10.2_{-8.2}^{+0.0} \times 10^{42}$	$4.1_{-2.3}^{+1.2} \times 10^{43}$
Te	$0.6_{-0.0}^{+3.4} \times 10^{42}$	$1.8_{-0.7}^{+1.0} \times 10^{43}$
Pt	$2.0_{-1.7}^{+0.0} \times 10^{42}$	$1.8_{-0.6}^{+0.3} \times 10^{43}$

TABLE I. Energy generation rate densities of UH-UHECRs, allowed by the two composition models used in this work.

because of much smaller statistical errors in the measured flux and composition. Our results are summarized in Table I.

In Fig. 2, we provide the results of our fitting for the energy spectrum and composition of UHECRs measured by Auger [76, 77] (see SM for details). With *Model A* and *Model B*, we see that the energy generation rate density of the three UH nuclear species is constrained to be

$$Q_{\text{UH-UHECR}}^{\text{Auger}} \lesssim (0.3 - 15) \times 10^{42} \text{ erg Mpc}^{-3} \text{ yr}^{-1}. \quad (3)$$

The best-fit values derived from *Model B* can be about one order of magnitude smaller than those from *Model A*, because the presence of heavy iron-group nuclei gives tighter constraints on the fraction of UH-UHECRs. We note that the values have significant uncertainties, and more stringent constraints on the energy budget of UH-UHECRs are obtained when we use the best-fit models only with conventional nuclei (see SM for details).

The results for the TA data are shown in Fig. 2, where we find that the energy generation rate densities of UH-UHECRs are constrained to be

$$Q_{\text{UH-UHECR}}^{\text{TA}} \lesssim (1.1 - 5.7) \times 10^{43} \text{ erg Mpc}^{-3} \text{ yr}^{-1}, \quad (4)$$

for both composition models, which is about 3 times larger than that derived based on the Auger data for both composition models. In particular, we find that including UH-UHECRs as a second population can provide better fits to the observed energy spectrum and composition measured by TA with $\chi_{\text{min}}^2/\text{d.o.f.} \sim (0.2 - 0.25)$, compared to the fits only with conventional nuclei for both composition models, which give $\chi_{\text{min}}^2/\text{d.o.f.} \sim (0.3 - 0.4)$. Including additional UH-UHECRs does not lead to any improvement when fitting to Auger data with $\chi_{\text{min}}^2/\text{d.o.f.} \sim (2.2 - 2.9)$ (cf. $\chi_{\text{min}}^2/\text{d.o.f.} \sim (2.2 - 2.4)$ for the fits with only conventional nuclei). While UH-UHECRs help us better explain the highest-energy UHECR data, more conservatively, our results are also regarded as constraints on their possible contribution.

Recently, the TA Collaboration reported the detection of an extremely energetic UHECR event by the surface

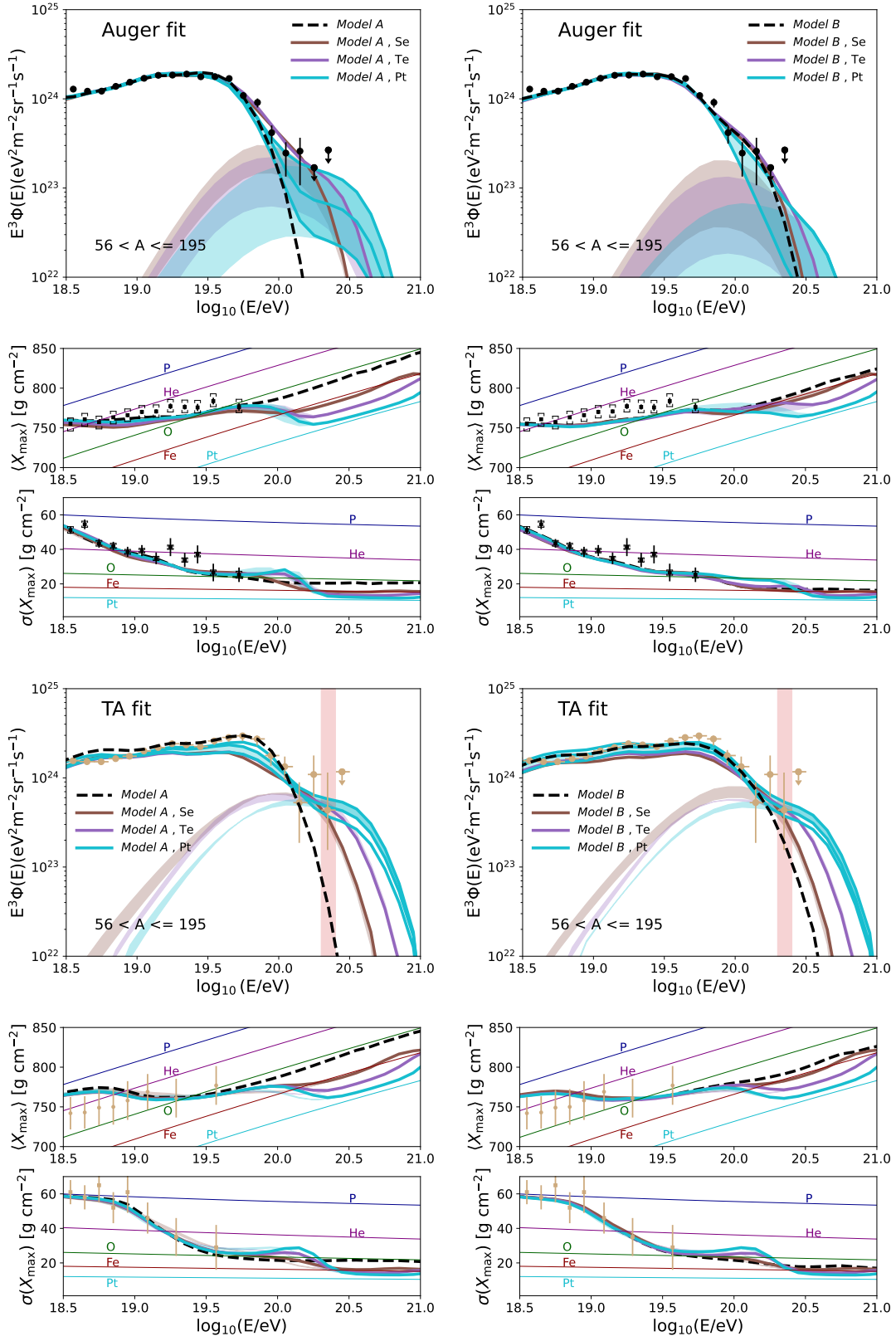


FIG. 2. Energy spectra and the first/second moments of X_{\max} distribution are shown considering both conventional and UH nuclei. Auger data are obtained from Refs. [76, 77], while TA data are from Refs. [78, 79]. Note that the data in the red vertical band corresponds to the Amaterasu particle [13].

detector, with an energy of about 244 EeV [13]. The nature of the particle is unclear at present. Even though the primary photon is excluded at the 99.985% confidence level, it is difficult to distinguish whether it is a proton or heavy nucleus [13]. Fig. 2 indicates that the Amaterasu particle may be explained as a UH-UHECR event. To explore this possibility, we also examine the backtracked direction of the Amaterasu particle for different nuclear species, as shown in Fig. 3, where we adopt the Galactic magnetic field model provided in Ref. [87]. For light or even iron nuclei, the direction of the Amaterasu particle lies in the local void region (yellow dotted curve in Fig. 3) [13, 88, 89]. If it is a UH nucleus, the source may exist outside the local void or even near the supergalactic plane thanks to the larger atomic number.

If UH-UHECRs contribute to the observed highest-energy cosmic rays, the required energy budget is $Q_{\text{UH-UHECR}} \sim 10^{43} \text{ erg Mpc}^{-3} \text{ yr}^{-1}$, which can be satisfied by both collapsars and BNS/NSBH mergers [34]. For example, the cosmic-ray luminosity density of BNS mergers is $\sim 10^{43.5} \text{ erg Mpc}^{-3} \text{ yr}^{-1}$, which is consistent with the kinetic energy $\mathcal{E}_{\text{ej}} \approx (1/2)M_{\text{ej}}c^2\beta_{\text{ej}}^2 \sim 2 \times 10^{51} \text{ erg} (M_{\text{ej}}/0.05 M_{\odot})(\beta_{\text{ej}}/0.2)^2$, the rate density $\rho \sim 300 \text{ Gpc}^{-3} \text{ yr}^{-1}$ [90, 91], and the energy fraction by cosmic rays, $\epsilon_{\text{CR}} \sim 5\%$. Short GRBs have isotropic-equivalent energies of $\mathcal{E}_{\gamma}^{\text{iso}} \sim 10^{51} - 10^{52} \text{ erg}$ and rate densities of $\rho \sim 10 \text{ Gpc}^{-3} \text{ yr}^{-1}$ [92, 93], inferring that the gamma-ray luminosity density is $\sim 10^{43} - 10^{44} \text{ erg Mpc}^{-3} \text{ yr}^{-1}$. Thus, it is possible for UH nuclei from BNS mergers and short GRBs to contribute to UHECRs above $\sim 10^{20} \text{ eV}$. The energy budget requirement for UH-UHECRs is less demanding, so collapsars such as long GRBs [94, 95] are also viable.

SUMMARY AND DISCUSSIONS

We presented the first detailed study on the propagation of UH-UHECRs, and derived general constraints on their contribution to the observed UHECR flux. Thanks to their energy loss lengths at $\lesssim 10^{21} \text{ eV}$, which are longer than those of protons and intermediate-mass nuclei, UH-UHECRs may significantly contribute to the highest-energy cosmic rays beyond $\sim 10^{20} \text{ eV}$, including the Amaterasu event. The allowed energy generation rate densities are consistent with those of collapsars and compact binary mergers [34].

Establishing the existence of UH nuclei at the highest energies may indicate that UHECRs are produced by transients rather than steady sources such as active galactic nuclei. UH nuclei as seeds for UHECRs can be synthesized in both BNS mergers and collapsars [23, 29, 47, 53]. Note that the UHECR acceleration should occur in outflows or ejecta [96] rather than at external forward shocks (e.g., Refs. [30, 32, 33]). Promising acceleration sites in-

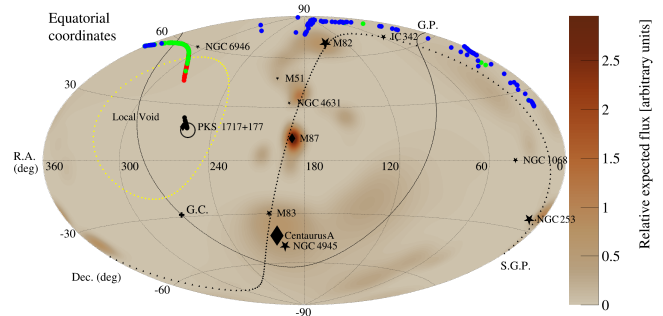


FIG. 3. Skymap of backtracked particles with mean energy $E = 244 \text{ EeV}$ and variation $E = 70 \text{ EeV}$ for p ($Z = 1$, black), Fe ($Z = 26$, red), Zr ($Z = 40$, green) and Pt ($Z = 78$, blue) in equatorial coordinates. For each nuclear species, we inject 100 particles. The arrival direction of the Amaterasu particle is (R.A., Dec.) = $(255.9 \pm 0.6^\circ, 16.1 \pm 0.5^\circ)$ in equatorial coordinates, indicated as a black circle. The black circle indicates the arrival direction of the Amaterasu particle. The supergalactic plane (S.G.P.) is shown as black dotted curves, and the Galactic plane (G.P.) is shown as black solid curves. The color bar represents the expected relative flux from sources in the local large-scale structure. This figure is generated with the code provided by Ref. [13].

clude external reverse shocks [20, 27] or internal dissipation [20, 28, 71]. More detailed implications for the sources, including the nucleus survival problem, will be discussed in future work [63].

The UH nuclear origin of UHECRs could be tested with future measurements of the composition at the highest energies, as indicated in Figs. 2. This behavior is in contrast to a high-luminosity GRB model that predicts a lighter composition at the highest energies [26] and a reacceleration model that changes toward an iron-group composition [32]. Multimessenger observations with neutrinos and gamma rays would also be useful. This scenario also requires the survival of nuclei inside the sources, in which TeV gamma rays are likely to escape from the sources [20]. Neutrinos may come from beta decay of nuclei [65], while the gamma-ray signal from nuclear deexcitation and electromagnetic cascades induced by the Bethe-Heitler process could be interesting targets for future gamma-ray detectors such as the Cherenkov Telescope Array [22].

We thank Toshihiro Fujii, Kunihito Ioka, Michael Unger, and Xilu Wang for useful information and discussions. This work was supported by NSF Grants Nos. AST-1908689 (K.M. and M.B.) and AST-1908960 (N.E., M.B. and S.H.). We also acknowledge NSF Grants Nos. AST-2108466 (K.M.), AST-2108467 (K.M.), AST-2308021 (K.M.), and PHY-2209420 (S.H.), and U.S. DOE Office of Science award number DE-SC0020262 (S.H.), and KAKENHI Nos. 20H01901 (K.M. and B.T.Z.), 20H05852 (K.M. and B.T.Z.), 22K03630 (S.H.), and 23H04899 (S.H.). M.B. acknowledges support from

the Eberly Postdoctoral Fellowship at the Pennsylvania State University. This work was supported by World Premier International Research Center Initiative (WPI Initiative), MEXT, Japan.

Note added. — While the paper was being finalized, a related work [97] appeared. Our work is independent and focuses on the general aspects of UH-UHECRs that can be produced by not only BNS mergers but also collapsars.

-
- [1] A. M. Hillas, The Origin of Ultrahigh-Energy Cosmic Rays, *Ann. Rev. Astron. Astrophys.* **22**, 425 (1984).
- [2] M. Nagano and A. A. Watson, Observations and implications of the ultrahigh-energy cosmic rays, *Rev. Mod. Phys.* **72**, 689 (2000).
- [3] K. Kotera and A. V. Olinto, The Astrophysics of Ultrahigh Energy Cosmic Rays, *Ann. Rev. Astron. Astrophys.* **49**, 119 (2011), arXiv:1101.4256 [astro-ph.HE].
- [4] R. Alves Batista *et al.*, Open Questions in Cosmic-Ray Research at Ultrahigh Energies, *Front. Astron. Space Sci.* **6**, 23 (2019), arXiv:1903.06714 [astro-ph.HE].
- [5] R. U. Abbasi *et al.* (HiRes Collaboration), First observation of the Greisen-Zatsepin-Kuzmin suppression, *Phys. Rev. Lett.* **100**, 101101 (2008), arXiv:astro-ph/0703099 [astro-ph].
- [6] J. Abraham *et al.* (Pierre Auger Collaboration), Observation of the suppression of the flux of cosmic rays above 4×10^{19} eV, *Phys. Rev. Lett.* **101**, 061101 (2008), arXiv:0806.4302 [astro-ph].
- [7] J. Abraham *et al.* (Pierre Auger Collaboration), Measurement of the energy spectrum of cosmic rays above 10^{18} eV using the Pierre Auger Observatory, *Phys. Lett.* **B685**, 239 (2010), arXiv:1002.1975 [astro-ph.HE].
- [8] D. Ivanov (Telescope-Array, Pierre Auger), Report of the Telescope Array - Pierre Auger Observatory Working Group on Energy Spectrum, PoS **ICRC2017**, 498 (2018).
- [9] A. Aab *et al.* (Pierre Auger), The Pierre Auger Cosmic Ray Observatory, *Nucl. Instrum. Meth. A* **798**, 172 (2015), arXiv:1502.01323 [astro-ph.IM].
- [10] H. Tokuno *et al.*, New air fluorescence detectors employed in the Telescope Array experiment, *Nucl. Instrum. Meth. A* **676**, 54 (2012), arXiv:1201.0002 [astro-ph.IM].
- [11] T. Abu-Zayyad *et al.* (Telescope Array), The surface detector array of the Telescope Array experiment, *Nucl. Instrum. Meth. A* **689**, 87 (2013), arXiv:1201.4964 [astro-ph.IM].
- [12] D. R. Bergman *et al.* (Pierre Auger, Telescope Array), Measurement of UHECR energy spectrum with the Pierre Auger Observatory and the Telescope Array, PoS **ICRC2023**, 406 (2024).
- [13] R. U. Abbasi *et al.* (Telescope Array), An extremely energetic cosmic ray observed by a surface detector array, *Science* **382**, abo5095 (2023), arXiv:2311.14231 [astro-ph.HE].
- [14] A. A. Halim *et al.* (Pierre Auger), Constraining the sources of ultra-high-energy cosmic rays across and above the ankle with the spectrum and composition data measured at the Pierre Auger Observatory, *JCAP* **05**, 024, arXiv:2211.02857 [astro-ph.HE].
- [15] K. Greisen, Cosmic ray showers, *Ann. Rev. Nucl. Part. Sci.* **10**, 63 (1960).
- [16] J. Abraham *et al.* (Pierre Auger), Measurement of the Depth of Maximum of Extensive Air Showers above 10^{18} eV, *Phys. Rev. Lett.* **104**, 091101 (2010), arXiv:1002.0699 [astro-ph.HE].
- [17] A. Aab *et al.* (Pierre Auger), Depth of Maximum of Air-Shower Profiles at the Pierre Auger Observatory: Measurements at Energies above $10^{17.8}$ eV, *Phys. Rev. D* **90**, 122005 (2014), arXiv:1409.4809 [astro-ph.HE].
- [18] A. Abdul Halim *et al.* (Pierre Auger), Studies of the mass composition of cosmic rays and proton-proton interaction cross-sections at ultra-high energies with the Pierre Auger Observatory, PoS **ICRC2023**, 438 (2023).
- [19] A. Abdul Halim *et al.* (Pierre Auger), Depth of maximum of air-shower profiles: testing the compatibility of the measurements at the Pierre Auger Observatory and the Telescope Array, PoS **ICRC2023**, 249 (2023).
- [20] K. Murase, K. Ioka, S. Nagataki, and T. Nakamura, High-energy cosmic-ray nuclei from high- and low-luminosity gamma-ray bursts and implications for multi-messenger astronomy, *Phys. Rev.* **D78**, 023005 (2008), arXiv:0801.2861 [astro-ph].
- [21] X.-Y. Wang, S. Razzaque, and P. Meszaros, On the Origin and Survival of UHE Cosmic-Ray Nuclei in GRBs and Hypernovae, *Astrophys. J.* **677**, 432 (2008), arXiv:0711.2065 [astro-ph].
- [22] K. Murase and J. F. Beacom, Very-High-Energy Gamma-Ray Signal from Nuclear Photodisintegration as a Probe of Extragalactic Sources of Ultrahigh-Energy Nuclei, *Phys. Rev.* **D82**, 043008 (2010), arXiv:1002.3980 [astro-ph.HE].
- [23] B. D. Metzger, D. Giannios, and S. Horiuchi, Heavy Nuclei Synthesized in Gamma-Ray Burst Outflows as the Source of UHECRs, *Mon. Not. Roy. Astron. Soc.* **415**, 2495 (2011), arXiv:1101.4019 [astro-ph.HE].
- [24] R.-Y. Liu and X.-Y. Wang, Energy spectrum and chemical composition of ultrahigh energy cosmic rays from semi-relativistic hypernovae, *Astrophys. J.* **746**, 40 (2012), arXiv:1111.6256 [astro-ph.HE].
- [25] S. Horiuchi, K. Murase, K. Ioka, and P. Meszaros, The survival of nuclei in jets associated with core-collapse supernovae and gamma-ray bursts, *Astrophys. J.* **753**, 69 (2012), arXiv:1203.0296 [astro-ph.HE].
- [26] B. T. Zhang, K. Murase, S. S. Kimura, S. Horiuchi, and P. Mészáros, Low-luminosity gamma-ray bursts as the sources of ultrahigh-energy cosmic ray nuclei, *Phys. Rev.* **D97**, 083010 (2018), arXiv:1712.09984 [astro-ph.HE].
- [27] B. T. Zhang and K. Murase, Ultrahigh-energy cosmic-ray nuclei and neutrinos from engine-driven supernovae, *Phys. Rev. D* **100**, 103004 (2019), arXiv:1812.10289 [astro-ph.HE].
- [28] D. Boncioli, D. Biehl, and W. Winter, On the common origin of cosmic rays across the ankle and diffuse neutrinos at the highest energies from low-luminosity Gamma-Ray Bursts, *Astrophys. J.* **872**, 110 (2019), arXiv:1808.07481 [astro-ph.HE].
- [29] M. Bhattacharya, S. Horiuchi, and K. Murase, On the synthesis of heavy nuclei in protomagnetar outflows and implications for ultra-high energy cosmic rays, *Mon. Not. Roy. Astron. Soc.* **514**, 6011 (2022), arXiv:2111.05863 [astro-ph.HE].

- [30] H. Takami, K. Kyutoku, and K. Ioka, High-Energy Radiation from Remnants of Neutron Star Binary Mergers, *Phys. Rev. D* **89**, 063006 (2014), arXiv:1307.6805 [astro-ph.HE].
- [31] K. Kyutoku and K. Ioka, The unreasonable weakness of r-process cosmic rays in the neutron-star-merger nucleosynthesis scenario, *Astrophys. J.* **827**, 83 (2016), arXiv:1603.00467 [astro-ph.HE].
- [32] S. S. Kimura, K. Murase, and P. Mészáros, Super-Knee Cosmic Rays from Galactic Neutron Star Merger Remnants, *Astrophys. J.* **866**, 51 (2018), arXiv:1807.03290 [astro-ph.HE].
- [33] X. Rodrigues, D. Biehl, D. Boncioli, and A. M. Taylor, Binary neutron star merger remnants as sources of cosmic rays below the “Ankle”, *Astropart. Phys.* **106**, 10 (2019), arXiv:1806.01624 [astro-ph.HE].
- [34] K. Murase and M. Fukugita, Energetics of High-Energy Cosmic Radiations, *Phys. Rev. D* **99**, 063012 (2019), arXiv:1806.04194 [astro-ph.HE].
- [35] B. Katz, R. Budnik, and E. Waxman, The energy production rate & the generation spectrum of UHECRs, *JCAP* **0903**, 020, arXiv:0811.3759 [astro-ph].
- [36] Y. Jiang, B. T. Zhang, and K. Murase, Energetics of ultrahigh-energy cosmic-ray nuclei, *Phys. Rev. D* **104**, 043017 (2021), arXiv:2012.03122 [astro-ph.HE].
- [37] R. D. Blandford, Acceleration of ultrahigh-energy cosmic rays, *Phys. Scripta T* **85**, 191 (2000), arXiv:astro-ph/9906026.
- [38] E. M. Burbidge, G. R. Burbidge, W. A. Fowler, and F. Hoyle, Synthesis of the elements in stars, *Rev. Mod. Phys.* **29**, 547 (1957).
- [39] F. K. Thielemann, M. Eichler, I. V. Panov, and B. Wehmeyer, Neutron Star Mergers and Nucleosynthesis of Heavy Elements, *Ann. Rev. Nucl. Part. Sci.* **67**, 253 (2017), arXiv:1710.02142 [astro-ph.HE].
- [40] C. J. Horowitz *et al.*, r-Process Nucleosynthesis: Connecting Rare-Isotope Beam Facilities with the Cosmos, *J. Phys. G* **46**, 083001 (2019), arXiv:1805.04637 [astro-ph.SR].
- [41] T. Kajino, W. Aoki, A. B. Balantekin, R. Diehl, M. A. Famiano, and G. J. Mathews, Current status of r-process nucleosynthesis, *Prog. Part. Nucl. Phys.* **107**, 109 (2019), arXiv:1906.05002 [astro-ph.HE].
- [42] J. J. Cowan, C. Sneden, J. E. Lawler, A. Aprahamian, M. Wiescher, K. Langanke, G. Martínez-Pinedo, and F.-K. Thielemann, Origin of the heaviest elements: The rapid neutron-capture process, *Rev. Mod. Phys.* **93**, 15002 (2021), arXiv:1901.01410 [astro-ph.HE].
- [43] A. Arcones and F.-K. Thielemann, Origin of the elements, *Astron. Astrophys. Rev.* **31**, 1 (2023).
- [44] C. Freiburghaus, J.-F. Rembges, T. Rauscher, E. Kolbe, F.-K. Thielemann, K.-L. Kratz, B. Pfeiffer, and J. J. Cowan, The astrophysical r-process: A comparison of calculations following adiabatic expansion with classical calculations based on neutron densities and temperatures, *The Astrophysical Journal* **516**, 381 (1999).
- [45] S. Wanajo, Y. Sekiguchi, N. Nishimura, K. Kiuchi, K. Kyutoku, and M. Shibata, Production of all the r-process nuclides in the dynamical ejecta of neutron star mergers, *Astrophys. J. Lett.* **789**, L39 (2014), arXiv:1402.7317 [astro-ph.SR].
- [46] I. Bartos and S. Marka, A nearby neutron-star merger explains the actinide abundances in the early Solar System, *Nature* **569**, 85 (2019).
- [47] N. Ekanger, M. Bhattacharya, and S. Horiuchi, Nucleosynthesis in outflows of compact objects and detection prospects of associated kilonovae, *Mon. Not. Roy. Astron. Soc.* **525**, 2040 (2023), arXiv:2303.00765 [astro-ph.HE].
- [48] S. Fujibayashi, K. Kiuchi, S. Wanajo, K. Kyutoku, Y. Sekiguchi, and M. Shibata, Comprehensive Study of Mass Ejection and Nucleosynthesis in Binary Neutron Star Mergers Leaving Short-lived Massive Neutron Stars, *Astrophys. J.* **942**, 39 (2023), arXiv:2205.05557 [astro-ph.HE].
- [49] D. M. Siegel, J. Barnes, and B. D. Metzger, Collapsars as a major source of r-process elements, *Nature* **569**, 241 (2019), arXiv:1810.00098 [astro-ph.HE].
- [50] J. Barnes and B. D. Metzger, Signatures of r-process Enrichment in Supernovae from Collapsars, *Astrophys. J. Lett.* **939**, L29 (2022), arXiv:2205.10421 [astro-ph.HE].
- [51] N. Nishimura, T. Takiwaki, and F. K. Thielemann, The r-process nucleosynthesis in the various jet-like explosions of magnetorotational core-collapse supernovae, *Astrophys. J.* **810**, 109 (2015), arXiv:1501.06567 [astro-ph.SR].
- [52] D. Yong *et al.*, r-Process elements from magnetorotational hypernovae, *Nature* **595**, 223 (2021), arXiv:2107.03010 [astro-ph.SR].
- [53] N. Ekanger, M. Bhattacharya, and S. Horiuchi, Systematic exploration of heavy element nucleosynthesis in protomagnetar outflows, *Mon. Not. Roy. Astron. Soc.* **513**, 405 (2022), arXiv:2201.03576 [astro-ph.HE].
- [54] S. Zha, B. Müller, and J. Powell, Nucleosynthesis in the Innermost Ejecta of Magnetorotational Supernova Explosions in 3-dimensions (2024), arXiv:2403.02072 [astro-ph.HE].
- [55] M. Reichert, M. Bugli, J. Guilet, M. Obergaulinger, M. A. Aloy, and A. Arcones, Nucleosynthesis in magnetorotational supernovae: impact of the magnetic field configuration, *Mon. Not. Roy. Astron. Soc.* **529**, 3197 (2024), arXiv:2401.14402 [astro-ph.HE].
- [56] R. Alves Batista *et al.*, CRPropa 3.2 — an advanced framework for high-energy particle propagation in extragalactic and galactic spaces, *JCAP* **09**, 035, arXiv:2208.00107 [astro-ph.HE].
- [57] A. J. Koning, S. Hilaire, and M. C. Duijvestijn, TALYS: Comprehensive Nuclear Reaction Modeling, *AIP Conf. Proc.* **769**, 1154 (2005).
- [58] Koning, A. J., Hilaire, S., and Duijvestijn, M. C., TALYS-1.0, *International Conference on Nuclear Data for Science and Technology*, 211 (2007).
- [59] NuDat 3 Data Base, National Nuclear Data Center (NNDC), Brookhaven National Laboratory, Upton, NY, USA, <https://www.nndc.bnl.gov/nudat3/>.
- [60] R. C. Gilmore, R. S. Somerville, J. R. Primack, and A. Dominguez, Semi-analytic modeling of the EBL and consequences for extragalactic gamma-ray spectra, *Mon. Not. Roy. Astron. Soc.* **422**, 3189 (2012), arXiv:1104.0671 [astro-ph.CO].
- [61] F. W. Stecker, Photodisintegration of ultrahigh-energy cosmic rays by the universal radiation field, *Phys. Rev.* **180**, 1264 (1969).
- [62] J. L. Puget, F. W. Stecker, and J. H. Bredekamp, Photonuclear Interactions of Ultrahigh-Energy Cosmic Rays and their Astrophysical Consequences, *Astrophys. J.* **205**, 638 (1976).
- [63] N. Ekanger *et al.*, in preparation.

- [64] S. Karakula and W. Tkaczyk, The formation of the cosmic ray energy spectrum by a photon field, *Astropart. Phys.* **1**, 229 (1993).
- [65] K. Murase and J. F. Beacom, Neutrino Background Flux from Sources of Ultrahigh-Energy Cosmic-Ray Nuclei, *Phys. Rev.* **D81**, 123001 (2010), arXiv:1003.4959 [astro-ph.HE].
- [66] K. Murase, F. Oikonomou, and M. Petropoulou, Blazar Flares as an Origin of High-Energy Cosmic Neutrinos?, *Astrophys. J.* **865**, 124 (2018), arXiv:1807.04748 [astro-ph.HE].
- [67] K. Greisen, End to the cosmic ray spectrum?, *Phys. Rev. Lett.* **16**, 748 (1966).
- [68] G. T. Zatsepin and V. A. Kuzmin, Upper limit of the spectrum of cosmic rays, *JETP Lett.* **4**, 78 (1966), [*Pisma Zh. Eksp. Teor. Fiz.* **4**, 114(1966)].
- [69] F. W. Stecker, On the origin of the highest energy cosmic rays, *Phys. Rev. Lett.* **80**, 1816 (1998), arXiv:astro-ph/9710353.
- [70] F. W. Stecker and M. H. Salamon, Photodisintegration of ultrahigh-energy cosmic rays: A New determination, *Astrophys. J.* **512**, 521 (1999), arXiv:astro-ph/9808110.
- [71] B. T. Zhang, K. Murase, F. Oikonomou, and Z. Li, High-energy cosmic ray nuclei from tidal disruption events: Origin, survival, and implications, *Phys. Rev.* **D96**, 063007 (2017), arXiv:1706.00391 [astro-ph.HE].
- [72] K. Fang, K. Kotera, and A. V. Olinto, Newly-born pulsars as sources of ultrahigh energy cosmic rays, *Astrophys. J.* **750**, 118 (2012), arXiv:1201.5197 [astro-ph.HE].
- [73] K. Fang, K. Kotera, K. Murase, and A. V. Olinto, Testing the Newborn Pulsar Origin of Ultrahigh Energy Cosmic Rays with EeV Neutrinos, *Phys. Rev.* **D90**, 103005 (2014), arXiv:1311.2044 [astro-ph.HE].
- [74] D. Caprioli, "Espresso" Acceleration of Ultra-high-energy Cosmic Rays, *Astrophys. J.* **811**, L38 (2015), arXiv:1505.06739 [astro-ph.HE].
- [75] S. S. Kimura, K. Murase, and B. T. Zhang, Ultrahigh-energy Cosmic-ray Nuclei from Black Hole Jets: Recycling Galactic Cosmic Rays through Shear Acceleration, *Phys. Rev. D* **97**, 023026 (2018), arXiv:1705.05027 [astro-ph.HE].
- [76] A. Aab *et al.* (Pierre Auger), Measurement of the cosmic-ray energy spectrum above 2.5×10^{18} eV using the Pierre Auger Observatory, *Phys. Rev. D* **102**, 062005 (2020), arXiv:2008.06486 [astro-ph.HE].
- [77] A. Yushkov (Auger), Mass Composition of Cosmic Rays with Energies above $10^{17.2}$ eV from the Hybrid Data of the Pierre Auger Observatory, *PoS ICRC2019*, 482 (2020).
- [78] J. Kim *et al.* (Telescope Array), Highlights from the Telescope Array Experiment, *PoS ICRC2023*, 008 (2024).
- [79] R. U. Abbasi *et al.* (Telescope Array), Depth of Ultra High Energy Cosmic Ray Induced Air Shower Maxima Measured by the Telescope Array Black Rock and Long Ridge FADC Fluorescence Detectors and Surface Array in Hybrid Mode, *Astrophys. J.* **858**, 76 (2018), arXiv:1801.09784 [astro-ph.HE].
- [80] M. Lemoine, Extra-galactic magnetic fields and the second knee in the cosmic-ray spectrum, *Phys. Rev. D* **71**, 083007 (2005), arXiv:astro-ph/0411173.
- [81] V. Berezhinsky and A. Z. Gazizov, Diffusion of Cosmic Rays in the Expanding Universe. 2. Energy Spectra of Ultra-High Energy Cosmic Rays, *Astrophys. J.* **669**, 684 (2007), arXiv:astro-ph/0702102.
- [82] A. A. Halim *et al.* (Pierre Auger), Impact of the Magnetic Horizon on the Interpretation of the Pierre Auger Observatory Spectrum and Composition Data (2024), arXiv:2404.03533 [astro-ph.HE].
- [83] K. Murase and H. Takami, Implications of Ultra-High-Energy Cosmic Rays for Transient Sources in the Auger Era, *Astrophys. J. Lett.* **690**, L14 (2009), arXiv:0810.1813 [astro-ph].
- [84] H. Takami and K. Murase, The Role of Structured Magnetic Fields on Constraining Properties of Transient Sources of Ultra-high-energy Cosmic Rays, *Astrophys. J.* **748**, 9 (2012), arXiv:1110.3245 [astro-ph.HE].
- [85] T. Pierog, I. Karpenko, J. M. Katzy, E. Yatsenko, and K. Werner, EPOS LHC: Test of collective hadronization with data measured at the CERN Large Hadron Collider, *Phys. Rev. C* **92**, 034906 (2015), arXiv:1306.0121 [hep-ph].
- [86] K. Murase, C. D. Dermer, H. Takami, and G. Migliori, Blazars as Ultra-High-Energy Cosmic-Ray Sources: Implications for TeV Gamma-Ray Observations, *Astrophys. J.* **749**, 63 (2012), arXiv:1107.5576 [astro-ph.HE].
- [87] R. Jansson and G. R. Farrar, The Galactic Magnetic Field, *Astrophys. J. Lett.* **761**, L11 (2012), arXiv:1210.7820 [astro-ph.GA].
- [88] M. Unger and G. R. Farrar, Where Did the Amaterasu Particle Come From?, *Astrophys. J. Lett.* **962**, L5 (2024), arXiv:2312.13273 [astro-ph.HE].
- [89] M. Y. Kuznetsov, A nearby source of ultra-high energy cosmic rays, *JCAP* **04**, 042, arXiv:2311.14628 [astro-ph.HE].
- [90] R. Abbott *et al.* (KAGRA, VIRGO, LIGO Scientific), Population of Merging Compact Binaries Inferred Using Gravitational Waves through GWTC-3, *Phys. Rev. X* **13**, 011048 (2023), arXiv:2111.03634 [astro-ph.HE].
- [91] N. Sarin, P. D. Lasky, F. H. Vivanco, S. P. Stevenson, D. Chattopadhyay, R. Smith, and E. Thrane, Linking the rates of neutron star binaries and short gamma-ray bursts, *Phys. Rev. D* **105**, 083004 (2022), arXiv:2201.08491 [astro-ph.HE].
- [92] D. Wanderman and T. Piran, The rate, luminosity function and time delay of non-Collapsar short GRBs, *Mon. Not. Roy. Astron. Soc.* **448**, 3026 (2015), arXiv:1405.5878 [astro-ph.HE].
- [93] A. R. Escorial *et al.*, The Jet Opening Angle and Event Rate Distributions of Short Gamma-Ray Bursts from Late-time X-Ray Afterglows, *Astrophys. J.* **959**, 13 (2023), arXiv:2210.05695 [astro-ph.HE].
- [94] M. Milgrom and V. Usov, Possible association of ultrahigh-energy cosmic ray events with strong gamma-ray bursts, *Astrophys. J.* **449**, L37 (1995), arXiv:astro-ph/9505009 [astro-ph].
- [95] E. Waxman, Cosmological origin for cosmic rays above 10^{19} -eV, *Astrophys. J.* **452**, L1 (1995), arXiv:astro-ph/9508037 [astro-ph].
- [96] The transrelativistic SN model [27] predicts that the maximal rigidity is similar among sources, which is consistent with the recent analysis [98], because gamma rays are produced in a different region.
- [97] G. R. Farrar, Binary neutron star mergers as the source of the highest energy cosmic rays (2024), arXiv:2405.12004 [astro-ph.HE].
- [98] D. Ehlert, F. Oikonomou, and M. Unger, Curious

- case of the maximum rigidity distribution of cosmic-ray accelerators, *Phys. Rev. D* **107**, 103045 (2023), arXiv:2207.10691 [astro-ph.HE].
- [99] N. Globus, A. Fedynitch, and R. D. Blandford, Treasure Maps for Detections of Extreme Energy Cosmic Rays, *Astrophys. J.* **945**, 12 (2023), arXiv:2210.15885 [astro-ph.HE].
- [100] E. Khan, S. Goriely, D. Allard, E. Parizot, T. Suomijarvi, A. J. Koning, S. Hilaire, and M. C. Duijvestijn, Photodisintegration of ultra-high-energy cosmic rays revisited, *Astropart. Phys.* **23**, 191 (2005), arXiv:astro-ph/0412109 [astro-ph].
- [101] M. Unger, G. R. Farrar, and L. A. Anchordoqui, Origin of the ankle in the ultrahigh energy cosmic ray spectrum, and of the extragalactic protons below it, *Phys. Rev.* **D92**, 123001 (2015), arXiv:1505.02153 [astro-ph.HE].
- [102] K. A. Olive *et al.* (Particle Data Group), Review of Particle Physics, *Chin. Phys.* **C38**, 090001 (2014).
- [103] K. Fang and K. Murase, Linking High-Energy Cosmic Particles by Black Hole Jets Embedded in Large-Scale Structures, *Nature Phys.* **14**, 396 (2018), arXiv:1704.00015 [astro-ph.HE].
- [104] A. Aab *et al.* (Pierre Auger), Combined fit of spectrum and composition data as measured by the Pierre Auger Observatory, *JCAP* **04**, 038, [Erratum: *JCAP* 03, E02 (2018)], arXiv:1612.07155 [astro-ph.HE].
- [105] P. Plotko, A. van Vliet, X. Rodrigues, and W. Winter, Differences between the Pierre Auger Observatory and Telescope Array Spectra: Systematic Effects or Indication of a Local Source of Ultra-high-energy Cosmic Rays?, *Astrophys. J.* **953**, 129 (2023), arXiv:2208.12274 [astro-ph.HE].
- [106] K. Murase, Ultrahigh-Energy Photons as a Probe of Nearby Transient Ultrahigh-Energy Cosmic-Ray Sources and Possible Lorentz-Invariance Violation, *Phys. Rev. Lett.* **103**, 081102 (2009), arXiv:0904.2087 [astro-ph.HE].
- [107] S. Marafico, J. Biteau, A. Condorelli, O. Deligny, and J. Bregeon, Closing the net on transient sources of ultra-high-energy cosmic rays, (2024), arXiv:2405.17179 [astro-ph.HE].

SUPPLEMENTAL MATERIAL

Interactions of UH Nuclei

Photodisintegration cross sections for UH nuclei derived from TALYS 1.96 are shown in Fig. 4. We also show the photodisintegration cross section of iron nuclei for comparison. We see a reasonably good match between the analytical estimate and the numerical results. In Fig. 5, we show the energy loss length for three typical UH nuclei, namely Selenium (Se), Tellurium (Te), and Platinum (Pt), respectively.

To study the change in the composition of UH-UHECRs during propagation, we estimate the fraction of survived nuclei $f_{\text{survival}} = N_{\text{obs}}(E > E_{\text{obs}}, A > A_{\text{obs}}) / N_{\text{inj}}(E_{\text{inj}})$ numerically with CRPROPA 3 [e.g., 99], where N_{inj} is the number of nuclei injected at a given distance, N_{obs} is the observed number of particles, A_{obs} and E_{obs} are the observed nuclei mass number and energy, respectively. The propagation distance $d_{95\%}$ can be inferred when the value of $f_{\text{survival}} = 5\%$, which implies that 95% of the nuclei are lost during propagation. In Fig. 6, we show the propagation distance $d_{95\%}$ for three typical UH nuclei species. For UH nuclei with primary energy $E_{\text{inj}} = 300$ EeV, the propagation distance is $d_{95\%} \sim 1.5$ Mpc for Se ($A_{\text{obs}} \geq 80$), $d_{95\%} \sim 6.5$ Mpc for Te ($A_{\text{obs}} \geq 130$) and $d_{95\%} \sim 7.5$ Mpc for Pt ($A_{\text{obs}} \geq 195$). The propagation distance increases to $d_{95\%} \approx 65$ Mpc for Se ($A_{\text{obs}} \geq 56$), $d_{95\%} \approx 320$ Mpc for Te ($A_{\text{obs}} \geq 56$) and $d_{95\%} \approx 480$ Mpc for Pt ($A_{\text{obs}} \geq 56$).

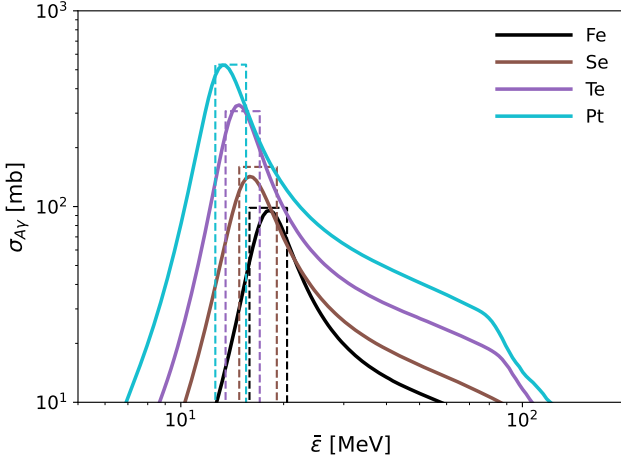


FIG. 4. Photodisintegration cross sections for UH nuclei as a function of photon energy in the nuclear rest frame. Solid curves are from the output of TALYS 1.96, while the dashed boxes are estimated using the rectangular approximation [63].

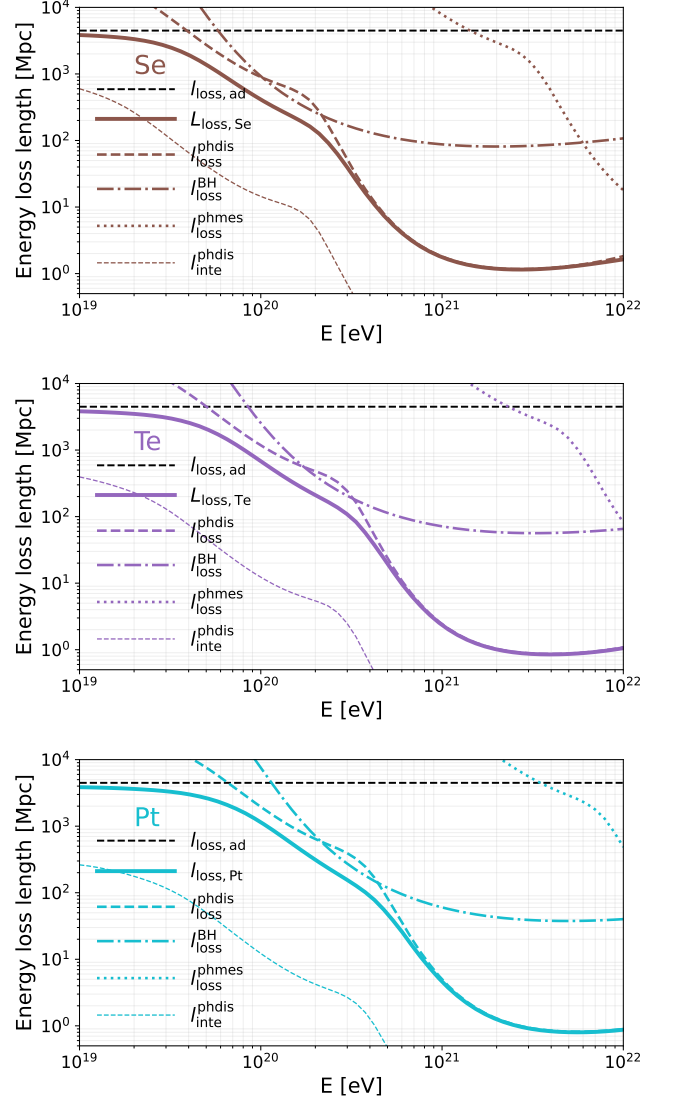


FIG. 5. Energy loss lengths for photodisintegration (thick dashed lines), photomeson production (dotted lines), Bethe-Heitler pair production (dotted-dashed lines), and adiabatic expansion (black-dashed line) of UH nuclei of Se, Te, and Pt, as a function of nuclear energy. We also indicate interaction lengths for the photodisintegration process (thin dashed lines).

Fitting Procedure

Here, we describe the details of the fitting procedure for the observed UHECR spectra and composition. The observed flux is estimated with the following formula [e.g., 71],

$$\Phi_A = \sum_{A'} \Phi_{AA'} = \sum_{A'} \frac{c}{4\pi} \frac{dn_{AA'}}{dE}, \quad (5)$$

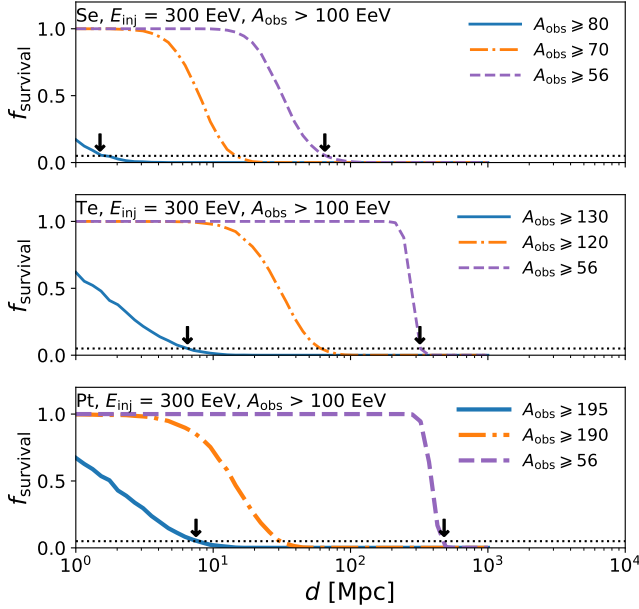


FIG. 6. Propagation distance, $d_{95\%}$, corresponding to $f_{\text{survival}} = 5\%$, is shown for Se, Te, and Pt. The black-dashed lines correspond to a value of 0.05 indicating that 95% of the nuclei are lost during propagation.

and

$$dn_{AA'}(E) = \int_{z_{\min}}^{z_{\max}} dz \left| \frac{dt}{dz} \right| \xi(z) \times \int_{E'_{\min}}^{E'_{\max}} dE' \frac{d\dot{N}_{A'}}{dE'} \eta_{AA'}(E, E', z), \quad (6)$$

where $\eta_{AA'}(E, E', z)$ is a factor representing the number of secondary UHECRs with mass number A and energy E that are generated from parent nuclei with the mass number A' and E' [71, 100, 101], z is redshift, $\xi(z)$ is the redshift evolution factor, and $dt/dz = -1/[H_0(1+z)(\sqrt{\Omega_\Lambda + \Omega_k(1+z)^2} + \Omega_m(1+z)^3)]$. We assume a continuous source distribution with a minimum source distance of $d_{\min} = 1.5$ Mpc and a maximum source distance of $d_{\max} = 3854$ Mpc, corresponding to redshifts, $z_{\min} = 0.0003$ and $z_{\max} = 4.5$, respectively. Note that the distances, d_{\min} and d_{\max} , should be treated as light travel distances. The minimum injection energy is $E'_{\min} = 10^{18}$ eV, and the maximum injection energy is $E'_{\max} = 10^{21}$ eV. The cosmological parameters adopted in this work are $H_0 = 67.3$ km s $^{-1}$ Mpc $^{-1}$, $\Omega_m = 0.315$, $\Omega_\Lambda = 0.685$, and $\Omega_k = 0$ [102].

We adopt the chi-square method to fit the observed energy spectrum and composition [36], and use

$$\chi_{\text{spec}}^2 = \sum_i \frac{(f\Phi^{\text{model}}(\hat{E}_i; s_{\text{CR}}, \mathcal{R}_{\max}) - \Phi(E_i))^2}{\Delta(\Phi)_i^2} + \left(\frac{\delta_E}{\sigma_E} \right)^2, \quad (7)$$

where f is a free normalization parameter, Φ^{model} is the simulation results, $\hat{E}_i \equiv (1 + \delta_E)E_i$, $\Delta(\Phi)$ is the statistic uncertainty, and σ_E is the systematic uncertainty on the measured energy scale by Auger ($\sigma_E \sim 14\%$) [76] and TA ($\sigma_E \sim 21\%$) [78]. In this work, the systematic uncertainty on the energy scale is not considered by setting $\delta_E = 0$. We note that the variation of the observed flux $E^3\Phi$ has an uncertainty of $\sim 30\%$ ($\sim 50\%$) for Auger (TA) [14]. Correspondingly, our constraints on the energy generation rate densities of UH-UHECRs in Table I and Table IV would be subject to this systematics.

Similarly, we estimate the χ^2 value when fitting to the composition. For the first and second moments of X_{\max} distribution, $\langle X_{\max} \rangle$ and $\sigma(X_{\max})$, we have

$$\chi_{\langle X_{\max} \rangle}^2 = \sum_i \frac{(\langle X_{\max}^{\text{model}} \rangle(\hat{E}_i; s_{\text{CR}}, \mathcal{R}_{\max}) - \langle X_{\max} \rangle(E_i))^2}{\Delta(X_{\max})_i^2}, \quad (8)$$

$$\chi_{\sigma(X_{\max})}^2 = \sum_i \frac{(\sigma(X_{\max})^{\text{model}}(\hat{E}_i; s_{\text{CR}}, \mathcal{R}_{\max}) - \sigma(X_{\max})(E_i))^2}{\Delta(\sigma(X_{\max}))_i^2}, \quad (9)$$

where $\Delta(X_{\max})$ and $\Delta(\sigma(X_{\max}))$ are the uncertainties including both statistical and systematic uncertainties [e.g., 103]. The total χ^2 value is

$$\chi^2 = \chi_{\text{spec}}^2 + \chi_{\langle X_{\max} \rangle}^2 + \chi_{\sigma(X_{\max})}^2, \quad (10)$$

and the best-fit results are obtained when χ^2 reaches its minimum value χ_{\min}^2 . In this work, we fit the observed spectrum and composition with energies above $10^{18.75}$ eV for Auger data. There are 16 data points for the spectrum and 20 data points for the moments of the X_{\max} distribution. For TA data, we consider energies above $10^{18.45}$ eV, with 21 data points on the spectrum and 18 data points for the moments of the X_{\max} distribution. The degree of freedom (d.o.f.) is defined as the total number of data points minus the number of fitting parameters. We treat the maximum particle energy (\mathcal{R}_{\max}), spectral index (s_{CR}), energy generation rate density (Q_{UHECR}), and number fraction of nuclei (f_A), as the free parameters. Note that $\sum f_A = 1$, generated as the direction cosines in k dimensions using the same method described in Ref. [104]. In Table II, we show the best-fit parameters used in Fig. 2.

Constraints from the Best-Fit Models Only with Conventional Nuclei

We constrain the energy generation rate density of UH-UHECRs, $Q_{\text{UH-UHECR}}$, based on the best-fit model using only conventional nuclei. Specifically, we begin with the best-fit results considering only conventional nuclei,

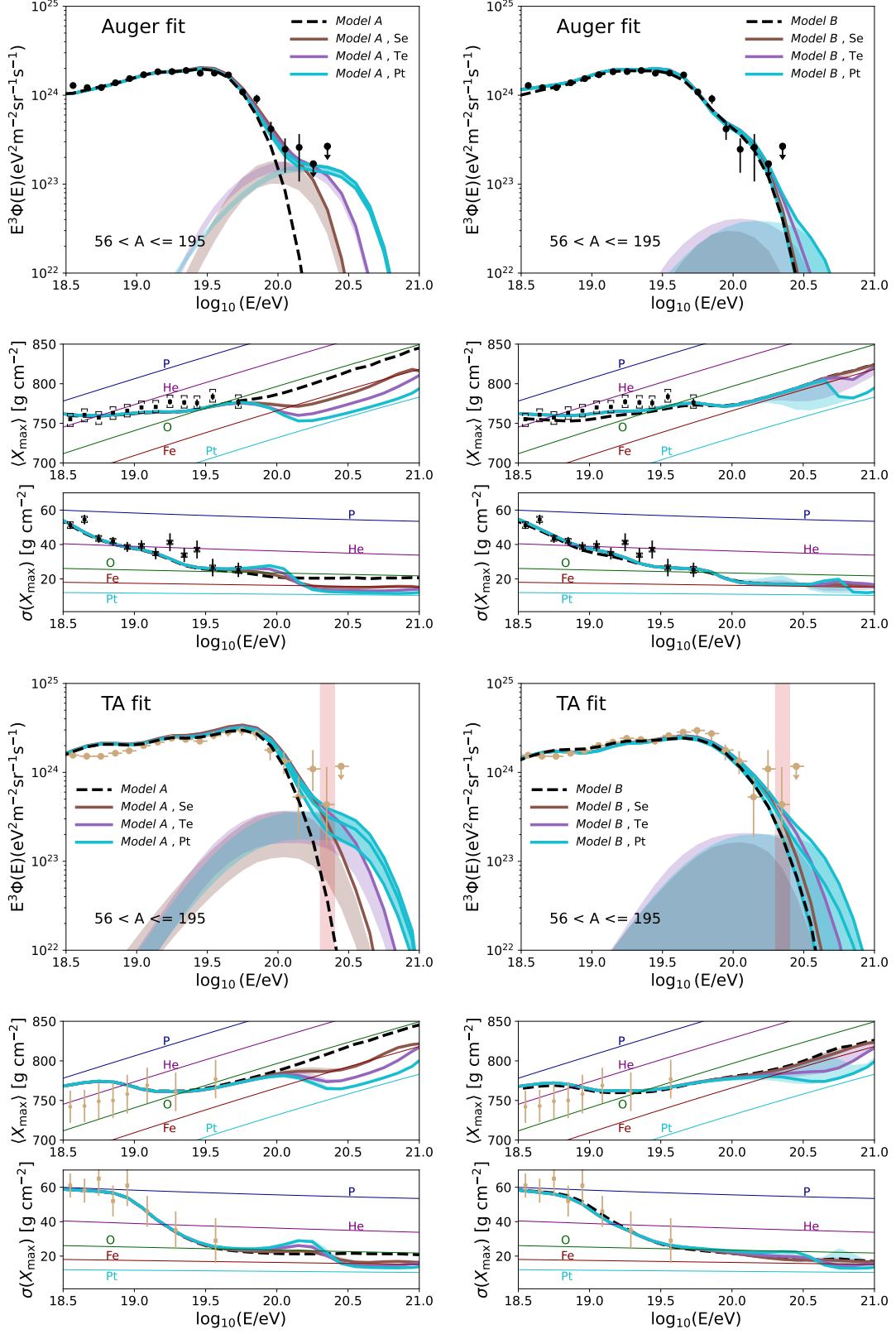


FIG. 7. Energy spectra and the first/second moments of X_{\max} distribution considering both conventional and UH nuclei. Auger data are obtained from Refs. [76, 77], while TA data are from Refs. [78, 79].

	<i>Model A</i> (+ Se)	<i>Model A</i> (+ Te)	<i>Model A</i> (+ Pt)	<i>Model B</i> (+ Se)	<i>Model B</i> (+ Te)	<i>Model B</i> (+ Pt)
Auger						
Q_{44}	4.7	4.9	5.3	4.9	4.9	4.7
\mathcal{R}_{\max}	$10^{18.3}$	$10^{18.3}$	$10^{18.2}$	$10^{18.2}$	$10^{18.2}$	$10^{18.3}$
s_{CR}	-0.3	-0.4	-1.1	-0.8	-0.7	-0.3
f_{P}	3.4%	24.52%	10.5%	2.1%	15.5%	17.8%
f_{He}	0.8%	3.1%	30.5%	25.6%	29.45%	0.09%
f_{O}	87.0%	64.2%	52.4%	68.1%	48.1%	74.3%
f_{Si}	8.1%	8.1%	6.57%	3.1%	5.74%	6.57%
f_{Fe}	-	-	-	0.7%	1.2%	1.2%
f_{Se}	0.7%	-	-	0.4%	-	-
f_{Te}	-	0.08%	-	-	0.01%	-
f_{Pe}	-	-	0.03%	-	-	0.04%
TA						
Q_{44}	6.3	6.4	6.1	6.4	6.8	6.8
\mathcal{R}_{\max}	$10^{18.7}$	$10^{18.5}$	$10^{18.7}$	$10^{18.7}$	$10^{18.7}$	$10^{18.7}$
s_{CR}	0.4	0.4	0.4	0.4	0.5	0.5
f_{P}	25.1%	28.8%	39.1%	39.0%	35.2%	44.0%
f_{He}	5.7%	0.2%	6.0%	15.94%	32.7%	5.8%
f_{O}	36.3%	22.8%	4.5%	19.4%	1.2%	19.5%
f_{Si}	31.3%	47.6%	50.1%	24.5%	30.4%	30.5%
f_{Fe}	-	-	-	0.02%	0.2%	0.003%
f_{Se}	1.6%	-	-	1.14%	-	-
f_{Te}	-	0.6%	-	-	0.3%	-
f_{Pe}	-	-	0.3%	-	-	0.2%

TABLE II. Best-fit parameters used in Fig. 2, where $Q_{44} \equiv Q_{\text{UHECR}}/10^{44} \text{ erg Mpc}^{-3} \text{ yr}^{-1}$ and Q_{UHECR} is the total energy generation rate density including UH-UHECRs.

	<i>Model A</i> Auger	<i>Model B</i> Auger	<i>Model A</i> TA	<i>Model B</i> TA
Q_{44}	5.7	5.9	7.4	6.4
\mathcal{R}_{\max}	$10^{18.1}$	$10^{18.2}$	$10^{18.7}$	$10^{18.6}$
s_{CR}	-2.0	-1.3	0.2	0.0
f_{P}	0.8%	6.0%	0.4%	14.5%
f_{He}	53.15%	42.0%	4.9%	0.5%
f_{O}	41.5%	50.8%	0.2%	53.6%
f_{Si}	4.55%	0.1%	94.5%	27.3%
f_{Fe}	-	1.1%	-	4.1%

TABLE III. Best-fit parameters used in Fig. 7, where $Q_{44} \equiv Q_{\text{UHECR}}/10^{44} \text{ erg Mpc}^{-3} \text{ yr}^{-1}$.

summarized in Table III. Then, we inject UH-UHECRs as an additional source population, but with the same rigidity and spectral index. Our results are shown in Fig. 7. We can see that the obtained results provide more stringent constraints compared to the combined fit method, as shown in Table IV. With *Model A*, the energy generation rate densities of these three UH nuclei are constrained to be located in a narrow range, with $Q_{\text{UH-UHECR}}^{\text{Auger}} \sim (4 - 8) \times 10^{42} \text{ erg Mpc}^{-3} \text{ yr}^{-1}$. However, we only obtain the upper limits on the UH-UHECR energy budget when adopting *Model B*, $Q_{\text{UH-UHECR}}^{\text{Auger}} \lesssim (1.2 - 1.4) \times 10^{42} \text{ erg Mpc}^{-3} \text{ yr}^{-1}$. The reason is that including heavy iron-group nuclei provides a better fit for the observed energy spectra, with $\chi_{\text{tot,min}}/\text{d.o.f.} = 64/\text{d.o.f.}$

Nuclei	$Q_{\text{UH-UHECR}}^{\text{Auger}}$ [erg Mpc ⁻³ yr ⁻¹]	$Q_{\text{UH-UHECR}}^{\text{TA}}$ [erg Mpc ⁻³ yr ⁻¹]
<i>Model A</i> , fixed		
Se	$7.1^{+1.6}_{-2.1} \times 10^{42}$	$2.2^{+1.3}_{-1.1} \times 10^{43}$
Te	$5.7^{+0.0}_{-1.1} \times 10^{42}$	$1.7^{+0.4}_{-0.8} \times 10^{43}$
Pt	$5.0^{+0.0}_{-0.6} \times 10^{42}$	$1.5^{+0.4}_{-0.6} \times 10^{43}$
<i>Model B</i> , fixed		
Se	$\lesssim 1.6 \times 10^{42}$	$\lesssim (3.8 - 13) \times 10^{42}$
Te	$\lesssim 1.4 \times 10^{42}$	$\lesssim (4.8 - 11) \times 10^{42}$
Pt	$\lesssim 1.2 \times 10^{42}$	$\lesssim (4.7 - 9) \times 10^{42}$

TABLE IV. Energy generation rate densities of UH-UHECRs.

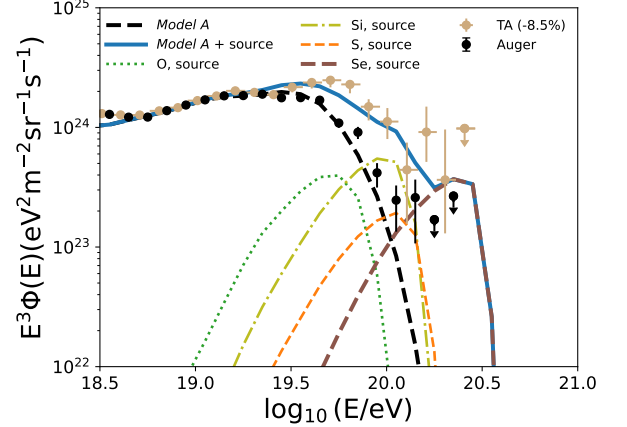


FIG. 8. Demonstrative example for explaining the TA spectrum with the best-fit model to the Auger data (*Model A*) with an additional contribution of UHECRs including UH nuclei from collapsars.

for conventional nuclei in *Model B* and $\chi_{\text{tot,min}}/\text{d.o.f.} = 72/\text{d.o.f.}$ in *Model A*, where d.o.f. is the degree of freedom. With TA data, we obtain $Q_{\text{UH-UHECR}}^{\text{TA}} \sim (1 - 3) \times 10^{43} \text{ erg Mpc}^{-3} \text{ yr}^{-1}$ for *Model A* and $Q_{\text{UH-UHECR}}^{\text{TA}} \lesssim (0.5 - 1.3) \times 10^{43} \text{ erg Mpc}^{-3} \text{ yr}^{-1}$ for *Model B*, which is about 3 times larger than that derived based on the Auger data.

Special Contribution from A Nearby Transient

A nearby transient may give a special contribution to the observed UHECR flux, and we explore the possibility of simultaneously explaining both the Auger and TA spectra. A specific example is shown in Fig. 8. The observed TA spectral excess may be affected by the systematic uncertainty on the energy scale, and we decrease the TA energy scale by a factor of 8.5% to match the Auger spectra in the low-energy range [12, 105]. Based on the best-fit model to the Auger data, we assume there are some nearby transient sources in the northern sky, mainly coming from the supergalactic plane, accounting for the spectral excess observed by TA. For demonstra-

tive purposes, we assume a nearby low-luminosity GRB located at $d = 5$ Mpc from Earth, and adopt the 16TJ model shown in Table I of Ref. [26] as the default composition model of nuclei, $f_O : f_{Si} : f_S = 0.52 : 0.37 : 0.11$, and the total injection UHECR luminosity above 10^{18} eV is $\mathcal{L}_{\text{UHECR}} \simeq 1.4 \times 10^{41}$ erg s $^{-1}$. Additionally, UH nuclei could be synthesized in the relativistic jet of GRBs [23, 29], where the most abundant UH nuclei can be the first-peak r -process elements such as Se, and the corresponding injection luminosity is $\mathcal{L}_{\text{UH-UHECR}} \simeq 1.4 \times 10^{40}$ erg s $^{-1}$. The typical delay time of UHECRs by the extragalactic magnetic field can be $\tau_d^{\text{EG}} \sim 1.7 \text{ yr} (Z/34)^2 E_{A,20.5}^{-2} B_{\text{EG},-11.5}^2 (l_c/1 \text{ Mpc})(d/5 \text{ Mpc})$,

where B_{EG} is the magnetic field strength that can be very weak in the void region, and d is source distance (e.g., Refs. [20, 106]). The Galactic magnetic field cause an inevitable time delay, $\tau_d^{\text{Gal}} \sim 200$ yr for a particle with rigidity 5 EV [83, 84, 107]. Thus, the total required energy of UHECRs emitted by a transient source is estimated to be $\mathcal{E}_{\text{UHECR}} \sim (\mathcal{L}_{\text{UHECR}} + \mathcal{L}_{\text{UH-UHECR}})(\tau_d^{\text{EG}} + \tau_d^{\text{Gal}}) \sim 9 \times 10^{50}$ erg, which can be consistent with cosmic-ray energy budgets of collapsars [20, 26, 27]. Note that even in this specific case our constraints on the energy generation rate density of UH-UHECRs still hold, and the results with the Auger data are applicable.